Check for updates

View Article Online
View Journal

INORGANIC CHEMISTRY

FRONTIERS

Accepted Manuscript

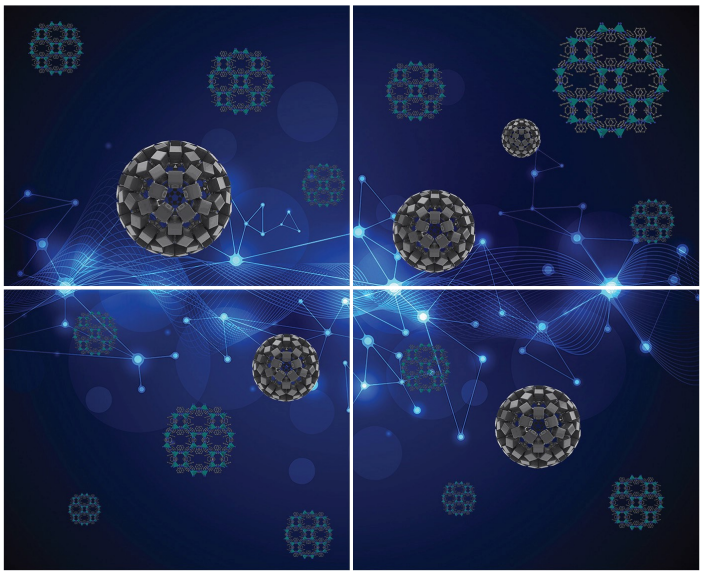

This article can be cited before page numbers have been issued, to do this please use: M. A. Pozo-López, R. Rojas Luna, S. Roy, F. J. Romero Salguero and D. Esquivel, *Inorg. Chem. Front.*, 2026, DOI: 10.1039/D6QI00603E.

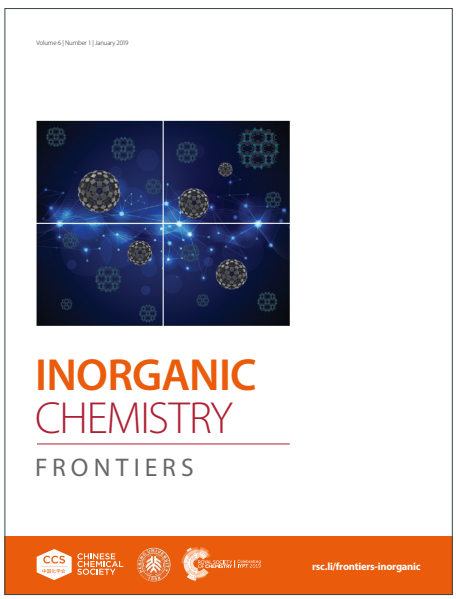

This is an Accepted Manuscript, which has been through the Royal Society of Chemistry peer review process and has been accepted for publication.

Accepted Manuscripts are published online shortly after acceptance, before technical editing, formatting and proof reading. Using this free service, authors can make their results available to the community, in citable form, before we publish the edited article. We will replace this Accepted Manuscript with the edited and formatted Advance Article as soon as it is available.

You can find more information about Accepted Manuscripts in the Information for Authors.

Please note that technical editing may introduce minor changes to the text and/or graphics, which may alter content. The journal's standard Terms & Conditions and the Ethical guidelines still apply. In no event shall the Royal Society of Chemistry be held responsible for any errors or omissions in this Accepted Manuscript or any consequences arising from the use of any information it contains.

View Article Online
DOI: 10.1039/D6QI00603E

ARTICLE

Open Access Article. Published on 22 June 2026. Downloaded on 6/23/2026 3:24:23 AM.
This article is licensed under a Creative Commons Attribution-NonCommercial 3.0 Unported Licence.

Covalent integration of photosensitizer and catalyst in the pore walls of periodic mesoporous organosilicas for efficient solar-driven CO_2 reduction

Received 00th January 20xx,
Accepted 00th January 20xx

DOI: 10.1039/x0xx00000x

Miguel A. Pozo-López,[a] Raúl Rojas-Luna,[b] Souvik Roy,[b] Francisco J. Romero-Salguero*[a] and Dolores Esquivel*[a]

Solid-state architectures that spatially integrate light-harvesting and catalytic sites offer a promising strategy for photocatalytic CO_2 reduction. However, most reported systems rely on metal–organic frameworks (MOFs), while analogous approaches using periodic mesoporous organosilicas (PMOs) remain unexplored. Herein, we report a dual-site periodic mesoporous organosilica (PMO) platform via co-immobilization of a visible-light photosensitizer (Ru- or Ir-based complexes) and a molecular CO_2 reduction catalyst, cobalt phthalocyanine (CoPc), within the pore walls of an ordered mesostructure. Under visible light irradiation, the PMO photosystems selectively convert CO_2 to CO, achieving cobalt-based turnover numbers, TON (CO), of 61 and 78 for CoPc-RuPMO and CoPc-IrPMO, respectively. These values significantly exceed those of immobilized CoPc with the sensitizers in solution, and are nearly one order of magnitude higher than CoPc on conventional semiconductor supports. Interestingly, a physical mixture of CoPc-ndppz and $Ru(bpy)_2Cl_2$ produces CO at similar rates, suggesting in situ formation of active Ru-based photosensitizers by self-assembly under reaction conditions. Photoluminescence quenching studies reveal rapid photoinduced electron transfer enabled by the close spatial proximity of the co-immobilized catalyst and sensitizer within the PMO scaffold and a reductive quenching pathway under the reaction conditions. These results demonstrate that spatially organized dual-site PMOs enable efficient photoinduced charge transfer, establishing them as versatile platforms for heterogeneous solar-driven CO_2 reduction.

Introduction

Ongoing global industrialization, accompanied by the ever-increasing energy demand, has led to a substantial increase in fossil fuels consumption.[1] Consequently, atmospheric CO_2 levels have risen significantly in recent decades, highlighting the urgent need for effective carbon mitigation strategies and the development of clean and sustainable energy sources.[2–8] Solar light-driven CO_2 reduction, which mimics natural photosynthesis, represents a promising approach for producing solar fuels and value-added chemical feedstocks, thereby offering a potential pathway to address both climate change and the global energy crisis.[9–14] Extensive research efforts have focused on the design of molecular systems incorporating transition metal complexes that function either as photosensitizers (PSs) - responsible for light absorption and electron transfer - , or as catalysts that use these electrons to drive CO_2 reduction reaction (CO_2RR). However, achieving high efficiency in such photocatalytic systems remains challenging, as performance is constrained not only by the intrinsic catalytic activity and the photophysical properties of the individual components, but also by the efficiency of electron transfer between them.[15–17] Over the past decade, numerous attempts have been conducted to strengthen the photoinduced electron transfer between PS and catalyst. Strategies such as hydrogen bonding, covalent linkage and coordinative interaction have been employed to construct effective electronic bridges between the two components, thereby facilitating charge separation and boosting CO_2 photoconversion.[18–20] Despite the enhanced photocatalytic performance achieved through these approaches, limited recyclability and long-term stability of these homogenous systems remain critical challenges, significantly restricting their practical applicability. In this context, the development of heterogeneous assemblies that integrate both PS and catalytic active sites have emerged as a promising strategy to overcome these drawbacks. Inorganic semiconductor-based systems, such as TiO_2 or ZrO_2, have shown great potential as heterogeneous catalysts for CO_2 photoreduction; however, their inherent absorption capacity is limited to the UV region. To extend their light-harvesting capability into the visible range and enhance CO_2 photoreduction efficiency, these materials typically require modification with visible-light absorbing sensitizers or co-dopants.[21–23] In response to these limitations, recent efforts have focused on the heterogenization of PS and molecular catalysts onto solid supports.[24–26] This approach aims to

[a] Departamento de Química Orgánica, Instituto Químico para la Energía y el Medio Ambiente (IQUEMA), Facultad de Ciencias, Universidad de Córdoba, Campus de Rabanales, 14071, Córdoba, Spain.
[b] School of Chemistry, University of Lincoln, Lincoln LN6 7DL, U.K.

† Supplementary Information available: [details of any supplementary information available should be included here]. See DOI: 10.1039/x0xx00000x

Inorganic Chemistry Frontiers Accepted Manuscript

View Article Online
DOI: 10.1039/D6QI00607F

Open Access Article. Published on 22 June 2026. Downloaded on 6/23/2026 3:24:23 AM. This article is licensed under a Creative Commons Attribution-NonCommercial 3.0 Unported Licence.

combine the high selectivity and tunability of homogenous catalysis with the robustness and recyclability of heterogenous systems, providing a promising pathway toward more efficient and sustainable CO_2 photoreduction.

Among the solid supports explored for the integration of PSs and catalytic units, metal-organic frameworks (MOFs)[27–29] and covalent-organic frameworks (COFs)[30,31] have attracted considerable attention in the field of CO_2 photocatalysis. These porous and crystalline materials meet key requirements for efficient CO_2RR. First, PS units are spatially distributed within the frameworks, therefore minimizing self-quenching effects and enhancing light-harvesting capacity. Second, the close proximity of PS molecules and catalytic sites embedded in the host matrix enables a rapid electron transfer from the excited or reduced PS to adjacent catalytic centers. Third, their beneficial textural properties, such as high surface areas and porosity, facilitate the diffusion of CO_2 molecules to the active sites. In addition to MOFs and COFs, periodic mesoporous organosilicas (PMOs) represent a compelling alternative as heterogenous platforms for anchoring PS and catalytic units. Their unique features - including well-defined ordered structures, large pore diameters, and functionalization of the organic moieties within pore walls - satisfy the demands of effective CO_2 photoreduction.[32] While MOF- and COF-based photocatalytic systems have been extensively studied for CO_2 photoreduction, only a few examples of PMOs are reported for this purpose, underscoring their untapped potential as a versatile platform for the hybrid photocatalyst design. In a pioneering study, Inagaki and co-workers developed the first photocatalytic system for CO_2 conversion by anchoring a Re-complex onto 2,2'-bipyridine ligands incorporated on the mesochannels of a photoactive biphenylene-bridged PMO.[33] In a similar approach, an enhanced photocatalytic activity was achieved when Re-bipyridyl complexes were immobilized on phenylene-bridged PMO nanotubes functionalized with bipyridine moieties.[34] More recent strategies have exploited bipyridine-bridged PMO (Bpy-PMO) as chelating platforms to heterogenize both the PS and the molecular catalyst, taking advantage of the strong coordination ability of bipyridyl ligands toward metal complexes.[35,36] Through this approach, both the Re-complex $[Re(bpy)(CO)_3]Cl$ (molecular catalyst) and the Ru-complex $[Ru(bpy)_3]^{2+}$ (photosensitizer) have been successfully embedded in the PMO framework via coordination with the bipyridyl ligands, affording efficient heterogeneous photocatalytic systems for CO_2 reduction.[37,38]

As an alternative to the Bpy-PMO support for generating well-defined organometallic sites, we recently reported the synthesis of a novel solid chelating platform, ndppz-PMO, prepared through the surfactant-directed self-assembly of a tailored home-made organosilane precursor containing dipyridylpyridazine units (ndppz) and 1,2-bis(triethoxysilyl)ethane. Ndppz-PMO was successfully employed as solid support for heterogenizing Ru- and Ir-complexes as photosensitizing units for photocatalytic hydrogen production.[39] Moreover, these N-chelating ligands have also been exploited to anchor Co- and Ni- based molecular catalysts bearing polypyridine ligands for CO_2 photoreduction in the presence of a homogenous photosensitizer,[40] and Ir-based complexes for chemical water oxidation reaction.[41] These findings clearly demonstrate the versatility of ndppz-PMO material, envisioned as a multifunctional platform for the heterogenization of both photosensitizing and catalytic units toward efficient H_2 and CO_2 conversion.

Herein, we report the synthesis of novel PMO-based hybrid photosystems that integrate both photosensitizer and molecular catalyst within a single, well-defined framework. By employing ndppz and cobalt-phthalocyanine (CoPc) organosilane precursors, followed by post-metalation with Ru and Ir complexes, we achieved precise spatial control over the distribution of the PS and the catalytic units in the PMO scaffold. CoPc was chosen as the catalyst because of its robustness and well-established CO_2 reduction properties, and accessibility to synthetic routes for integrating CoPc in PMOs.[42] Structural, textural and spectroscopic characterizations unambiguously confirmed the successful co-immobilization of both molecular components. Under visible-light irradiation, the resulting hybrid photosystems showed significantly enhanced CO_2 photoreduction activity compared to analogous photosystem containing immobilized catalyst (CoPc-ndppzPMO) and the non-surface-attached photosensitizer ($[Ru(bpy)_2(dppz)]^{2+}$ and $[Ir(ppy)_2(dppz)]^{+}$) in solution.

Experimental

Synthesis of CoPc-ndppzPMO

Periodic mesoporous organosilica containing cobalt phthalocyanine and 3,6-di-(2'-pyridyl)pyridazine moieties was synthesized according to the following procedure.[39] The structure-directing agent octadecyltrimethylammonium bromide (OTAB, 0.85 g) was dissolved in a basic solution consisting of distilled water (53 mL) and sodium hydroxide (6 M NaOH, 0.89 mL). The mixture was stirred at 40 °C for 24 h. Then, a mixture of organosilane precursors, containing the conventional bridged-organosilica source, 1,2-bis(triethoxysilyl)ethane (BTEE) (1.632 mmol), and the homemade ndppz trialkoxysilane precursor (0.408 mmol) was dissolved in 10 mL of DMSO containing $CoPc(SiOEt)_4$ (0.025 mmol) (see Supporting Information). This solution was then added dropwise to the reaction mixture under vigorous stirring. The resulting mixture was stirred at 40 °C for 24 h and subsequently aged at 97 °C for 5 days under static conditions. The resulting solid was collected by filtration and washed several times with water. To remove the surfactant from the pores, 1 g of as-synthesized material was refluxed overnight in 50 mL of ethanol containing 1 mL of HCl solution (37% wt). After repeating this extraction process twice, the solid was recovered by filtration, washed with ethanol and dried under vacuum at 80 °C to give CoPc-ndppzPMO (0.36 g) as a bluish-green powder.

Inorganic Chemistry Frontiers Accepted Manuscript

 This journal is © The Royal Society of Chemistry 20xx

Please do not adjust margins

View Article Online
DOI: 10.1039/D6QI00603E

Open Access Article. Published on 22 June 2026. Downloaded on 6/23/2026 3:24:23 AM.
This article is licensed under a Creative Commons Attribution-NonCommercial 3.0 Unported Licence.

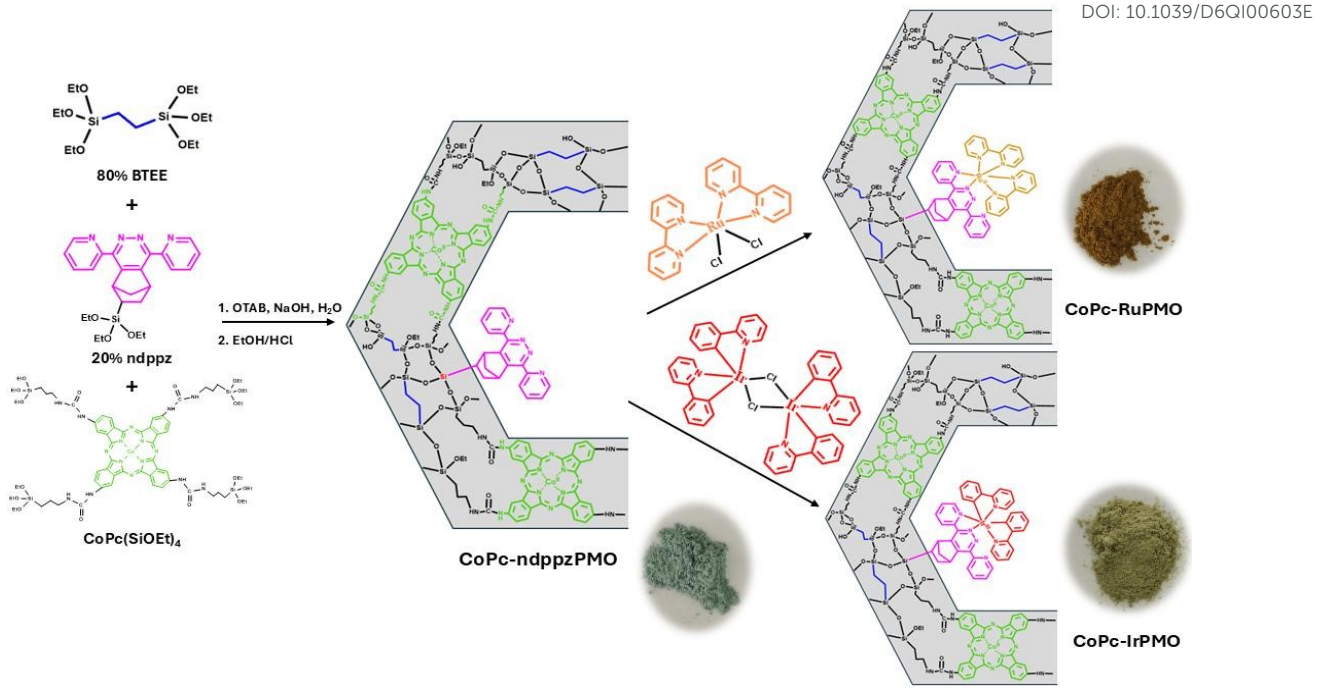

Scheme 1. Synthesis of CoPc-RuPMO and CoPc-IrPMO photocatalysts via post-synthetic metalation of CoPc-ndppzPMO.

Post-synthetic metalation of CoPc-ndppzPMO

Typically, CoPc-ndppzPMO (125 mg) was suspended in an ethanolic solution (40 mL) of $Ru(bpy)_2Cl_2$ (25 mg, 0.052 mmol) or in a dichloromethane solution (40 mL) of $Ir[(ppy)_2Cl]_2$ (25 mg, 0.024 mmol) to afford CoPc-RuPMO[43] and CoPc-IrPMO,[44] respectively. The resulting mixtures were stirred overnight at 80 °C. The solids were collected by filtration, washed with ethanol to remove any unreacted metal complex, and finally, dried under vacuum at 90 °C to yield CoPc-RuPMO as a brownish-yellow powder and CoPc-IrPMO as a greenish-yellow solid.

Photocatalytic experiments

Photocatalytic CO_2 reduction experiments were carried out in an 8 mL clear glass vial sealed with rubber septa. Typically, 1 mg of the photocatalyst (CoPc-RuPMO or CoPc-IrPMO) was dispersed in 4 mL CH_3CN/TEOA (9:1, v/v) solvent mixture containing 20 mM BIH as sacrificial electron donor. The mixture was purged with CO_2 for 20 min and irradiated with Xe Lamp (300 W) equipped with a water filter and Newport filter (FSQGC400, $\lambda \geq 400$ nm). Sample aliquots (50 µL) from the headspace were taken at different reaction times using a gas-tight syringe and quantified in a gas chromatograph (Shimadzu GC-2010 Plus) equipped with a barrier discharge ionization detector (BID) and a ShinCarbon ST column (2 m x 2 mm i.d.). After 9 h irradiation, 100 µL of reaction mixture was injected in high-performance liquid chromatograph (Agilent 1260 infinity II) equipped with a Hi-Plex column (300 x 7.7 mm) and a refractive index detector (RID) using H_2SO_4 (0.1 M) as mobile phase to determine any product present in the liquid phase.
Control experiments were performed under the same reaction conditions without one of the components: visible light, sacrificial electron donor (BIH), photosensitizer (without Ru and Ir complexes) or catalyst (without CoPc). Additionally, photocatalytic tests were carried out using CoPc-PMO catalyst without dppz coordinating units un the presence of $Ru(bpy)_2Cl_2$ or $Ir_2(ppy)_4Cl_2$ as photosensitizers under identical reaction conditions. For recycling experiments, 5 mg of the photocatalyst were irradiated for 6 h under identical conditions. After photocatalytic activity, the solid was collected by centrifugation and washed several times with acetonitrile to remove adsorbed compounds. Finally, the photocatalyst was redispersed again in a fresh CH_3CN/TEOA solution containing BIH (20 mM) and irradiated under the same reaction conditions.

Results and discussion

Synthesis and characterization

The heterogenization of both molecular units - catalyst and photosensitizer - within a single ordered scaffold for visible-light driven CO_2 photoreduction is presented in this study. For that, a dual-site periodic mesoporous organosilica (PMO) was synthesized via co-condensation of a cobalt phthalocyanine tetraalkoxysilane precursor with a bipyridine-like triethoxysilane precursor (ndppz). The former precursor enables the incorporation of the molecular catalyst (CoPc) into the silica framework, while the latter provides nitrogen-chelating ligands capable of coordinating metal complexes. Subsequent post-synthetic metalation of the dipyridylpyridazine moieties embedded within the pore walls with Ru and Ir precursors led to the formation of light-harvesting units, $[Ru(bpy)_2(dppz)]^{2+}$ and $[Ir(ppy)_2(dppz)]^{+}$, respectively. This metalation process is visually evidenced through a distinct color change from the initial bluish-green

Inorganic Chemistry Frontiers Accepted Manuscript

View Article Online
DOI: 10.1039/D6QI00607D

Open Access Article. Published on 22 June 2026. Downloaded on 6/23/2026 3:24:23 AM.
This article is licensed under a Creative Commons Attribution-NonCommercial 3.0 Unported Licence.

colour of CoPc-ndppz to a brownish-yellow or greenish-yellow color presented for CoPc-RuPMO or CoPc-IrPMO photocatalysts (Scheme 1).

The structural ordering of the materials was confirmed by powder X-ray diffraction (Fig. 1a). The XRD pattern of CoPc-ndppzPMO showed three diffraction peaks, one of high intensity at 2θ = 1.8° with d-spacing of 4.9 nm, and two weak peaks at higher incidence angles, associated with (100), (110) and (200) reflections, characteristics of a 2D-hexagonal material with a *p6mm* symmetry.[45] Similar XRD patterns were observed for the CoPc-RuPMO and CoPc-IrPMO photocatalysts, confirming that the original structure of CoPc-nppzPMO was preserved even after the formation of the photosensitizing units onto the pore surface. These results were further corroborated by HRTEM images (Fig. S6a and S6c), showing a regular hexagonal array of parallel mesochannel for both photocatalysts. Additionally, their corresponding FFT patterns (Fig. S6b and S6d) revealed multiple crystalline planes with d-spacing of 4.1 ± 0.5 nm and 2.1 ± 0.5 nm, corresponding to (100) and (110) reflections. These values are in good agreement with the results obtained from XRD analyses (Table S1).

The porous characteristics of these materials were evaluated by their nitrogen sorption isotherms at 77 K (Fig. 1b). All isotherms were type-IV with two-step capillary condensation at relative pressure (P/P_0 = 0.3 – 0.6), typical of mesoporous structures.[46] The textural properties are listed in Table S1. CoPc-ndppzPMO exhibited a Brunauer- Emmett–Teller specific surface area (S_{BET}) and total pore volume (V_p) of 860 $m^2\ g^{-1}$ and 0.72 $cm^3\ g^{-1}$, respectively. After metalation with Ru and Ir precursors, a significant decrease in both S_{BET} and V_p was observed, attributed to the partial clogging of the pores due to the assembly of $[Ru(bpy)_2(dppz)]^{2+}$ and $[Ir(ppy)_2(dppz)]^{+}$ moeities. CoPc-RuPMO and CoPc-IrPMO showed S_{BET} ranging from 720 to 750 $m^2\ g^{-1}$ and V_p between 0.55 and 0.60 $cm^3\ g^{-1}$. The pore size distribution profiles, calculated by non-local density functional theory (NDFT) method, are presented in Fig. 1c. CoPc-ndppzPMO showed a narrow pore size distribution with dominant mesopores centered at 3.8 nm, along with a minor population of smaller pores (< 2 nm). After metalation, the differential pore volume of the main mesopores decreased significantly, likely due to the coordination of Ru and Ir within the larger pores. Additionally, the pore size distribution peak exhibits a slight shift and broadening toward smaller pore sizes, further supporting the formation of light-harvesting units into the porous framework.

The presence of the molecular CoPc moieties integrated in the PMO framework was confirmed by FT-IR, Raman and UV-vis spectroscopies. FT-IR spectrum of $CoPc(SiOEt)_4$ precursor (Fig. 2a) displayed bands at 1533, 1411, 1272, 1161 and 788 cm^{-1} associated with the vibrations of isoindole groups of phthalocyanine ring, and a band at 952 cm^{-1} corresponding to Co-N stretching vibration, typical of metallophthalocyanines.[47] The presence of these bands for CoPc-ndppzPMO confirmed the successful incorporation of the CoPc catalytic units into the material. Moreover, additional peaks at 3461 and 1045 cm^{-1} were assigned to the hydroxyl stretching of the surface Si-OH groups and asymmetric stretching of Si-O-Si framework, respectively, generated as a result of the self-assembly co-condensation process.[48] Raman analysis of $CoPc(NH_2)_4$ and CoPc-ndppzPMO showed bands at 1600-1000 cm^{-1} characteristic of phthalocyanine skeletal vibrations (Fig. 2b).[47]

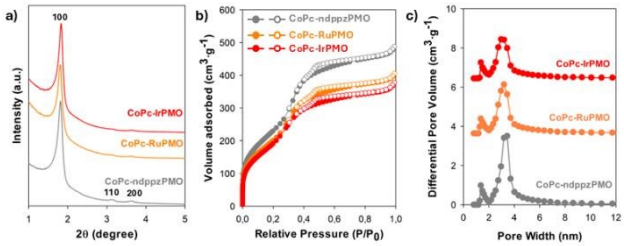

Fig. 1 (a) X-ray diffraction patterns of CoPc-ndppzPMO, CoPc-RuPMO and CoPc-IrPMO. (b) N_2 adsorption-desorption isotherms of materials. (c) Pore width distribution profiles for materials determined by NLDFT.

Two additional bands were observed at 800-600 cm^{-1} associated to stretching vibrations of Co-N, typical of metal phthalocyanines.[49] Additionally, the presence of CoPc units on CoPc-ndppzPMO were also confirmed by UV-Vis diffuse reflectance spectroscopy (DRS) which showed the characteristic B band ($S_0 \rightarrow S_2$) at 322 nm and the Q band ($S_0 \rightarrow S_1$) at 703 nm (Fig. 2c).[50] The noticeable peak broadening observed upon incorporation of the CoPc units into the silica framework can be attributed to the aggregation of phthalocyanine units within the ordered porous structures, as reported in materials such as COFs and PMOs.[51,52] In addition, a high-energy absorption band at ~ 280 nm, corresponding to the $\pi \rightarrow \pi^*$ electronic transition of the dipyridyl-pyridazine groups of the ndppz precursor, further confirms the incorporation of these N-chelating heterocyclic ligands in the support.[53] The formation of the light-harvesting units, $[Ru(bpy)_2(dppz)]^{2+}$ and $[Ir(ppy)_2(dppz)]^{+}$, in CoPc-RuPMO and CoPc-IrPMO photocatalysts upon metalation of the parent material with the corresponding metal precursors was also confirmed by UV-Vis DRS (Fig. 2d and 2e). In addition to the absorption bands previously observed by CoPc-ndppzPMO, the UV-vis spectrum of CoPc-RuPMO showed a broad band at 451 nm associated to the metal-to-ligand charge-transfer (MLCT) between the Ru center and bipyridine ligands.[54] This finding was supported by the presence of a similar absorption band in the UV-vis spectrum of the homogeneous $[Ru(bpy)_2(dppz)](PF_6)_2$ photosensitizer. In contrast, this MLCT band in the $Ru(bpy)_2Cl_2$ precursor appeared at a longer wavelength (~ 550 nm) due to the increased electron density at the Ru resulting from the coordination of the monodentate chloride ligands.[55] For CoPc-IrPMO photocatalyst, the UV-vis spectrum exhibited absorption bands in the range of 350 – 500 nm, associated to spin-allowed (~ 367 nm) and spin-forbidden (~ 465 nm) MLCT bands, respectively.[56] Similar absorption features were observed for the iridium dimer, and its respective homogeneous $[Ir(ppy)_2(dppz)]PF_6$ photosensitizer, confirming the successful coordination of the iridium complex to the surface dipyridyl-pyridazine units.[36,57]

Inorganic Chemistry Frontiers Accepted Manuscript

This journal is © The Royal Society of Chemistry 20xx

Please do not adjust margins

View Article Online
DOI: 10.1039/D6QI00603E

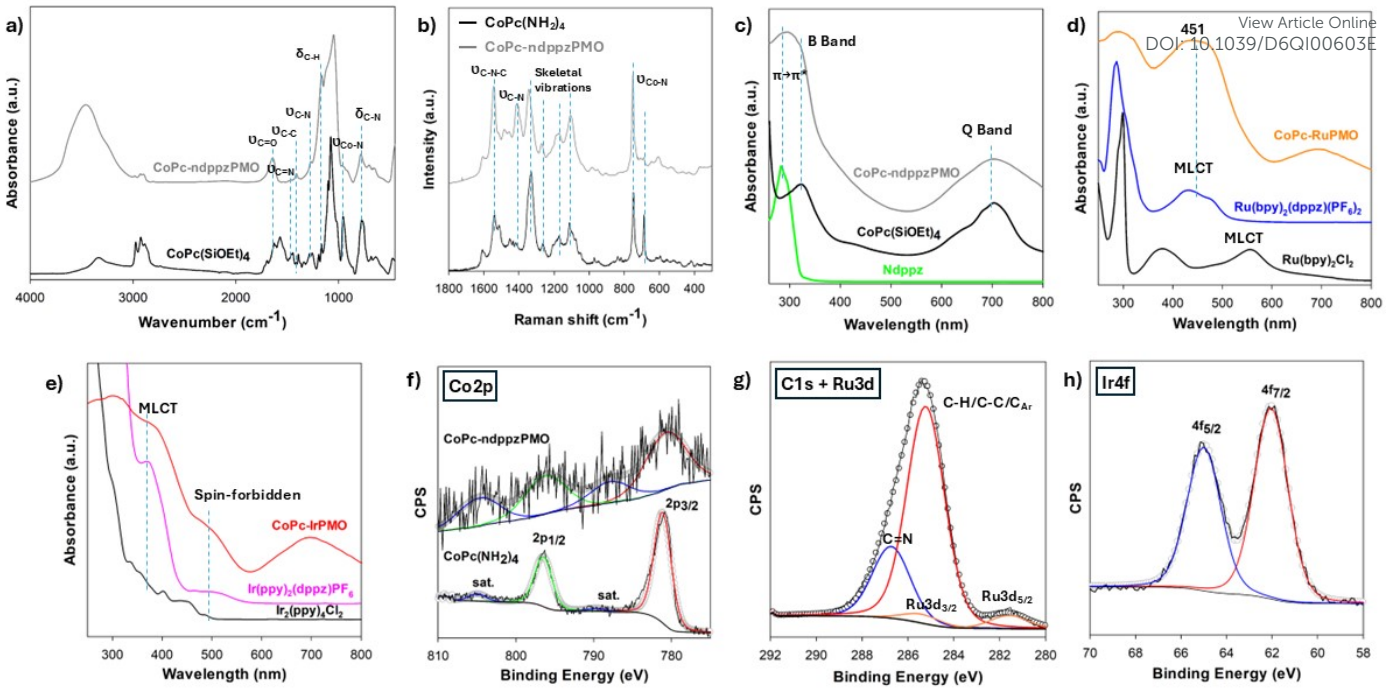

Fig. 2 (a) FT-IR spectra of $CoPc(SiOEt)_4$ and CoPc-ndppzPMO. (b) Raman spectra of $CoPc(NH_2)_4$ and CoPc-ndppzPMO. (c) UV-vis absorption spectra of ndppz (0.03 mM in EtOH) and $CoPc(SiOEt)_4$ (0.06 mM in DMSO) in solution and UV-vis diffuse reflectance spectrum of CoPc-ndppzPMO at solid-state. (d) UV-vis absorption spectra of $Ru(bpy)_2Cl_2$ (0.07 mM) and $Ru(bpy)_2(dppz)(PF_6)_2$ (0.04 mM) in CH_3CN and UV-Vis diffuse reflectance spectrum of CoPc-RuPMO at solid-state. (e) UV-vis absorption spectra of $Ir_2(ppy)_4Cl_2$ (0.03mM) and $Ir(ppy)_2(dppz)PF_6$ (0.2 mM) in CH_3CN and UV-vis diffuse reflectance spectrum of CoPc-IrPMO at solid-state. (f) Co 2p XPS spectra of $CoPc(NH_2)_4$ and CoPc-ndppzPMO. (g) C 1s + Ru 3d XPS spectrum of CoPc-RuPMO. (h) Ir 4f XPS spectrum of CoPc-IrPMO

The elemental composition and oxidation state of the metal species in the synthesized materials were evaluated by X-ray photoelectron spectroscopy (XPS). The survey spectra of all materials revealed the presence of Si, C, N, O and Co (Fig. S7). In addition, CoPc-RuPMO and CoPc-IrPMO displayed the presence of Ru and Ir, respectively. The Co 2p region of the phthalocyanine complex $CoPc(NH_2)_4$ (Fig. 2f) showed two distinct peaks at 781.3 and 796.5 eV, which correspond to the Co $2p_{3/2}$ and Co $2p_{1/2}$ transitions, along with two satellite features indicative of cobalt in +2 oxidation state.[58] Similar features were observed for the parent material and the corresponding photocatalysts, CoPc-RuPMO and CoPc-IrPMO (Fig. S8a and S8b), thus confirming the integration of the molecular catalyst in the organosilica framework. Moreover, the presence of the photosensitizing units in CoPc-RuPMO and CoPc-IrPMO were further verified via high-resolution C 1s + Ru 3d and Ir 4f XPS spectra, respectively. The C 1s + Ru 3d region (Fig. 2g) showed two main carbon contributions at 285.2 and 286.8 eV, corresponding to C-H/C-C/C_{ar} and C=N atoms, respectively,[39,42] previously observed for CoPc-ndppzPMO (Fig. S8c). Additionally, two new contributions centered at 281.5 and 285.6 eV were associated with the Ru $3d_{5/2}$ and Ru $3d_{3/2}$ spin-orbit components, respectively. These findings are consistent with the Ru^{2+} oxidation state.[59] Furthermore, the Ir 4f region for CoPc-IrPMO (Fig. 2h) showed two peaks at 62.1 and 65.0 eV assigned to Ir $4f_{7/2}$ and Ir $4f_{5/2}$, respectively, suggesting the presence of Ir^{3+}.[60]

The metal loadings in the samples were determined by inductively coupled plasma mass spectrometry (ICP-MS). While the Co loading remained unchanged for both photocatalysts (29.5 µmol Co g^{-1}), the precious metal loadings were different for CoPc-RuPMO (116 µmol Ru g^{-1}) and CoPc-IrPMO (83 µmol Ir g^{-1}), corresponding to a photosensitizer/catalyst molar ratio of approximately 3.9 and 2.8, respectively. Moreover, elemental mapping using energy dispersive X-ray spectroscopy (EDS) showed the homogeneous distribution of Co, Ru and Ir atoms throughout the material (Fig. S9).

Photocatalytic CO_2 reduction

Solar-driven CO_2RR experiments were carried out using CoPc-RuPMO or CoPc-IrPMO as a photocatalyst and BIH as a sacrificial electron donor under visible light. Headspace analysis by gas-chromatography revealed CO and H_2 as gaseous products, while no liquid products were detected by high-performance liquid chromatography.

Control tests were conducted to confirm the necessity of each component in the photocatalytic system (Fig. S10). In the absence of the catalytic CoPc units, RuPMO and IrPMO[39] - containing only photosensitizing units - produced only trace amounts of syngas. When the Ru and Ir complexes were omitted as photosensitizers, a negligible amount of syngas was observed in the presence of CoPc-ndppzPMO. Similarly, the removal of BIH from the system resulted in minimal syngas production, highlighting the crucial role of BIH as a two-electron donor that enables efficient electron transfer. Finally, to demonstrate the role of ndppz as chelating group, additional controls were performed using CoPc-PMO without dppz coordination units in combination with $Ru(bpy)_2Cl$ and $Ir_2(ppy)_4Cl_2$ as photosensitizers. After 6 hours of irradiation, both photosystems displayed lower catalytic activity, reaching a

Open Access Article. Published on 22 June 2026. Downloaded on 6/23/2026 3:24:23 AM.
This article is licensed under a Creative Commons Attribution-NonCommercial 3.0 Unported Licence.

Inorganic Chemistry Frontiers Accepted Manuscript

View Article Online DOI: 10.1039/D6QI00675

Open Access Article. Published on 22 June 2026. Downloaded on 6/23/2026 3:24:23 AM. This article is licensed under a Creative Commons Attribution-NonCommercial 3.0 Unported Licence.

total CO production of 112 and 355 µmol g^{-1}, respectively. Remarkably, CO selectivity decreased drastically to 20 and 52%, respectively, demonstrating the positive impact of ndppz chelating group within the same scaffold containing the catalytic units.

To elucidate the synergistic effect arising from the confinement of both heterogenized catalytic and photosensitizing units within the PMO framework, a reference photosystem was evaluated using CoPc-ndppzPMO as the catalyst and photosensitizers in solution ($[Ru(bpy)_2(dppz)](PF_6)_2$ and $[Ir(ppy)_2(dppz)]PF_6$) (see supplementary experimental section, Fig. S2-S5), at concentrations comparable to those in the corresponding heterogeneous photocatalysts (CoPc-RuPMO and CoPc-IrPMO). Electrochemical characterization (including cyclic voltammetry and redox potentials) and photophysical properties of these newly synthesized complexes are detailed in the Supporting Information (Fig. S11 and S12, and Table S2). As shown in Fig. 3a and c, photosystems with soluble photosensitizers, $[Ru(bpy)_2(dppz)]^{2+}$ or $[Ir(ppy)_2(dppz)]^{+}$, exhibited lower activity toward photocatalytic CO_2 reduction. CO production plateaued after 1 h of irradiation, yielding 280 ± 35 µmol g^{-1} and 183 ± 12 µmol g^{-1}, respectively. These values correspond to a Co-based TON(CO) of 9 for the Ru-based system and 6 for the Ir-based system. In both cases, photosystem deactivation was accompanied by the complete bleaching of the reaction mixture (Fig. 3a and c, inset), suggesting rapid photodecomposition of the photosensitizer in solution. Upon immobilizing the photosensitizing units into the PMO framework, the amount of CO produced by CoPc-RuPMO and CoPc-IrPMO after 1 h was comparable to their homogeneous photosystems. However, the co-immobilized photosystem displayed significantly improved longevity with sustained evolution of CO over longer time periods (Fig. 3b and d), with an initial reaction rate of 327 µmol g^{-1} h^{-1}, reaching a total CO production of 1820 ± 160 µmol CO g^{-1} for CoPc-RuPMO after 9 h. CoPc-Ir PMO displayed higher catalytic activity, producing 2310 ± 130 µmol g^{-1} of CO after 9 h with a reaction rate of 330 µmol g^{-1} h^{-1}. The lower activity for CoPc-RuPMO is due to the faster deactivation of the Ru-PS excited state arisen by the photodissociation of diimine ligands through the ^{3}MC (triplete metal-centered) state.[61] By contrast, for CoPc-IrPMO, cyclometalated ligands in the Ir-PS such as 2-phenylpyridine, increase ligand field stabilization energies, making the ^{3}MC state less accessible, which leads to longer lifetime of the Ir-PS excited state.[62,63]

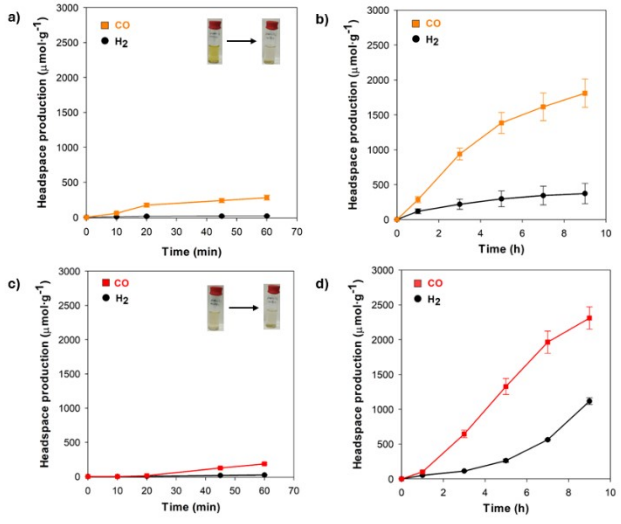

Fig. 3 Time-dependent CO (orange or red) and H_2 (black) evolution curves using (a) CoPc-ndppzPMO and 0.03 mM $[Ru(bpy)_2(dppz)]^{2+}$; (b) CoPc-RuPMO; (c) CoPc-ndppzPMO and 0.02 mM $[Ir(ppy)_2(dppz)]^{+}$, (d) and CoPc-IrPMO. Reaction conditions: 1 mg of CoPc-ndppzPMO, CoPc-RuPMO or CoPc-IrPMO, 4 mL mixture of CH_3CN/TEOA/ (9:1, v/v) and 20 mM BIH.

CoPc-RuPMO maintained a selectivity of up to 85% for CO production throughout the entire process. However, the CO selectivity for CoPc-IrPMO decreased from 82% to 67% over 9 h of irradiation. TON(CO) values for CoPc-RuPMO and CoPc-IrPMO photosystems were 61 and 78, respectively. These values are approximately 6.7 and 13-folds higher compared to those obtained with homogeneous photosensitizers under the same reaction conditions (*vide supra*). We hypothesise that there are two possible reasons behind the improved photocatalytic performance of CoPc-RuPMO and CoPc-IrPMO. First, immobilization of the photosensitizing units into the PMO scaffold increases durability by preventing the formation of deactivated Ru- and Ir-dimers. Second, the spatial proximity between Ru^{II} or Ir^{III} photosensitizers and Co^{II} catalytic sites within the ordered hybrid framework facilitates rapid and efficient electron transfer, thereby promoting the photocatalytic reduction of CO_2 to CO.

Following these findings, we compared our photocatalytic systems with previously reported heterogeneous photocatalysts based on cobalt-phthalocyanine as catalyst and carbon nitride as visible-light harvester in terms of CO production rate and TON (Table S3). Remarkably, our systems exhibited TON(CO) values nearly one order of magnitude higher than those previously reported,[58,64] reaching TON values comparable to state-of-the-art COF/C_3N_4 nanocomposites.[65]

To demonstrate the versatility and accessibility of the nitrogen-chelating ligands confined within the porous PMO channels for the construction of light-harvesting units, we also performed photocatalytic CO_2RR using CoPc-ndppzPMO and $Ru(bpy)_2Cl_2$ in a mixed solvent mixture CH_3CN/TEOA (9:1, v/v) with BIH. After stirring the reaction mixture in the dark for 1 h, the system was irradiated for 6 h. Under these conditions, the photocatalytic system reached a CO production of 1477 ± 86 µmol g^{-1}, which is comparable to that obtained for CoPc-RuPMO (Fig. 4a). This result suggests that $Ru(bpy)_2Cl_2$ rapidly coordinates with the dipyridyl-pyridazine (dppz) units embedded in the PMO framework, leading to the in-situ formation of the light-harvesting complex $[Ru(bpy)_2(dppz)]^{2+}$ within the pores. In contrast, under similar reaction conditions, the mixture of CoPc-ndppzPMO and $[Ir(ppy)_2Cl]_2$ showed markedly lower catalytic performance, yielding only 250 µmol g^{-1} after 6 h of irradiation (Fig. 4b). This poor performance suggests that Ir precursor is not able to coordinate the surface dipyridyl-pyridazine units under the reaction conditions. In addition, to confirm that the observed photocatalytic activity originated from the solid PMO-photocatalyst containing both catalytic and photosensitizing units, and not from the molecular

Inorganic Chemistry Frontiers Accepted Manuscript

This journal is © The Royal Society of Chemistry 20xx

Please do not adjust margins

View Article Online
DOI: 10.1039/D6QI00603E

species leached into solution, leaching tests were performed. The reaction mixture was irradiated for 3 h, after which the photocatalyst was removed by filtration and the resulting CO_2-saturated filtrate was then exposed to light for 3 h. No further CO generation was detected in either case (Fig. 4c and d), suggesting that the photocatalytic activity arises from the heterogenized photosystem and not from any species present in solution.

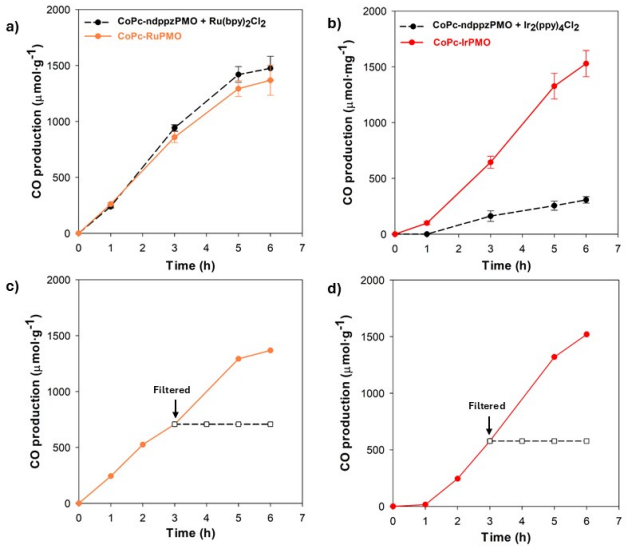

Fig. 4 In situ anchored experiments of (a) $Ru(bpy)_2Cl_2$ on CoPc-ndppzPMO and (b) $[Ir(ppy)_2Cl]_2$ on CoPc-ndppzPMO. Solid line shows normal behaviour of CoPc-RuPMO and CoPc-IrPMO and dashed line shows the activity of in situ formation of the photosensitizers. Leaching experiments for (c) CoPc-RuPMO and (d) CoPc-IrPMO. Solid line displays the normal course of the reaction using CoPc-RuPMO or CoPc-IrPMO and dashed line shows the activity of liquid phase after removing the catalyst.

To evaluate the photocatalytic stability of CoPc-RuPMO and CoPc-IrPMO, recycling tests were carried out (Fig. S13). After 6 h reaction, the photocatalysts were recovered by filtration, redispersed in a fresh reaction mixture, and irradiated under the same conditions. A significant decrease in catalytic activity (~ 50% of the initial CO production) was observed upon reuse. For CoPc-RuPMO, CO selectivity remained stable at 88%, whereas a decline in selectivity was noted by CoPc-IrPMO. ICP-MS analysis showed that approximately 75% of Co leached out from the photocatalysts in the first run, correlating with the observed loss of catalytic activity. Similar Co leaching from CoPc units was previously observed by our research group during catalytic turnover.[42] Furthermore, XRD patterns of the photocatalyst after 6 h of irradiation retained characteristic diffraction peaks of 2D-hexagonal structures, indicating that the ordered structures were maintained after catalysis (Fig. S14).

Mechanism of CO_2 photoreduction

Photophysical studies were performed to probe the CO_2 reduction mechanism by the hybrid materials. Time-resolved photoluminescence (TRPL) measurement was employed to evaluate the electron transfer between the PS and the CoPc units. The decay curves exhibited faster photoluminescence quenching in the solid materials with

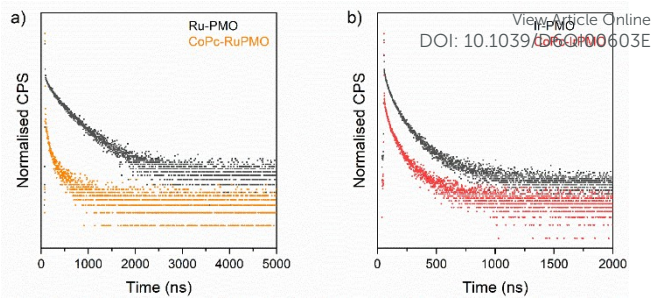

Fig. 5 Time-resolve photoluminescence spectra of (a) Ru-PMO and CoPc-RuPMO, and (b) Ir-PMO and CoPc-IrPMO.

embedded CoPc units (Fig. 5), indicating that electronic communication (via photoinduced electron transfer (PET) and/or energy transfer (EnT)) is facilitated by the proximity between the photosensitizer and the catalyst sites.[27] The average photoluminescence lifetime (τ) was estimated from the fitting of the decay curves using multi-exponential functions (Fig. S15). For the Ru-containing materials, the lifetime decreased from 358 to 138 ns, while for the Ir-based counterparts, a reduction from 87 to 44 ns was observed upon incorporation of CoPc. The presence of multiple lifetime components suggests different quenching environments, consistent with the heterogeneous nature of the sensitizing units.[37,66] This variation in quenching environments may arise from the spatially random molecular distribution of the immobilized sensitizer units on the PMO surface or within its channels, as well as their proximity to the embedded CoPc sites that can quench the photoexcited PS through oxidative electron transfer or energy transfer pathways. The emission decay for the homogeneous counterparts followed a monoexponential profile (Fig. S16), yielding lifetimes of 307 and 41 ns for $[Ru(bpy)_2(dppz)](PF_6)_2$ and $[Ir(ppy)_2(dppz)]PF_6$, respectively. The enhancement of the PS lifetime upon immobilization has also been reported in Metal-Organic Frameworks (MOFs).[27,67] This behavior is rationalized by the confinement effect within the pores, which restricts non-radiative decay pathways.

To evaluate the reductive quenching pathway, steady-state photoluminescence spectra were recorded with incremental equivalents of BIH as quencher. The emission of the photoexcited RuPMO and IrPMO was efficiently quenched upon addition of BIH (Fig. S17), suggesting that the excited state of Ru and Ir sensitizing units undergo deactivation by photoinduced electron transfer from BIH. Bimolecular quenching rate constant (kq) values of 5.8×10^8 M^{-1} s^{-1} (RuPMO) and 1.4×10^9 M^{-1} s^{-1} (IrPMO) were obtained from Stern-Volmer analysis (Fig. S18a and S18b). Nevertheless, photoluminescence emission of Ru and Ir was also significantly supressed upon integration of cobalt phthalocyanine units in the PMO scaffold (Fig. S19), with a decrease of emission intensity of 47% and 66% for CoPc-RuPMO and CoPc-IrPMO, respectively. This result, in line with TRPL analysis, indicates efficient intraframework communication between excited PS and catalytic units. While

Open Access Article. Published on 22 June 2026. Downloaded on 6/23/2026 3:24:23 AM.
This article is licensed under a Creative Commons Attribution-NonCommercial 3.0 Unported Licence.

Inorganic Chemistry Frontiers Accepted Manuscript

Please do not adjust margins

View Article Online
DOI: 10.1039/D6QI00603E

Open Access Article. Published on 22 June 2026. Downloaded on 6/23/2026 3:24:23 AM.
This article is licensed under a Creative Commons Attribution-NonCommercial 3.0 Unported Licence.

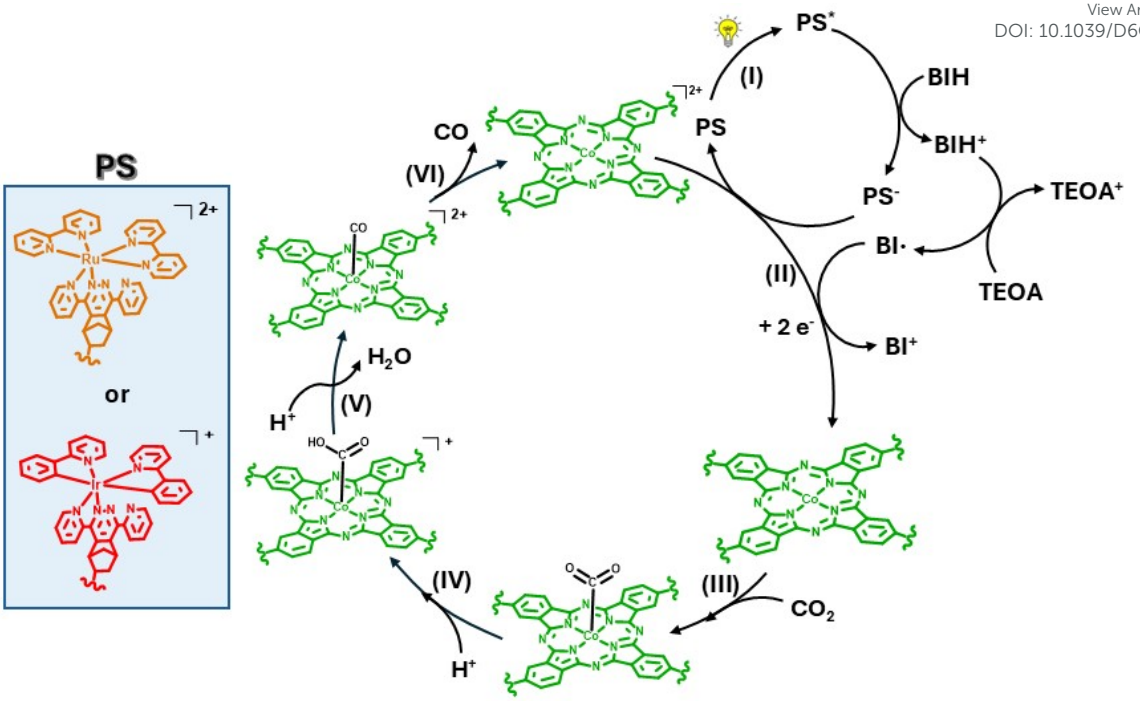

Scheme 2. Proposed mechanism for CO_2 photoreduction.

the spectral overlap between PS emission and the excitation at the CoPc Q-band (Fig. S20) suggests that a Förster-type EnT maycontribute to the quenching of PS,[68,69] these results also support the possibility of an oxidative quenching pathway through photoinduced electron transfer from Ru(II) and Ir(III) excited states to CoPc. Additionally, the incremental addition of BIH to CoPc-RuPMO and CoPc-IrPMO resulted in progressive quenching of the photoluminescence emission (Fig. S21), with k_q value of 1.6×10^9 M^{-1} s^{-1} (CoPc-RuPMO) and 1.9×10^9 M^{-1} s^{-1} (CoPc-IrPMO). These values exceeded those measured in the absence of CoPc moieties, indicating a more efficient quenching process in the fully integrated hybrid system.

Based on literature[70,71] and considering that the sacrificial electron donor is present in large excess ([BIH] = 20 mM), the calculated quenching efficiencies (η_q^{Ru} = 0.82; η_q^{Ir} = 0.63) support a photocatalytic mechanism governed predominantly by a reductive quenching pathway (Scheme 2). The process is initiated by absorption visible light by the integrated photosensitizer ($[Ru(bpy)_2(dppz)]^{2+}$ or $[Ir(ppy)_2(dppz)]^{+}$) (i). The excited photosensitizer is then reductively quenched by BIH, thus giving reduced photosensitizer and BIH^+. Subsequent deprotonation of BIH^+ generate BIH· radical, a highly reducing species capable of donating an additional electron. The two electrons (from PS^- and BI·) are rapidly transferred to a nearby CoPc unit (ii), followed by CO_2 coordination to the cobalt centre, leading to formation of $CoPc(CO_2)$ intermediate (iii). Protonation of these intermediate forms $[CoPc(COOH)^+]$ (iv), which subsequently undergoes a second protonation step, cleavage of C-O bond and elimination of a water molecule. This leads to formation of $[CoPc(CO)]^{2+}$ intermediate (v), which after release of CO, regenerates the catalyst (vi).

Conclusions

In conclusion, we have successfully synthesized two novel PMO-based photocatalysts, CoPc-RuPMO and CoPc-IrPMO, for solar-driven CO_2RR. Through a surfactant-directed self-assembly of two tailor-made organosilane precursors (ndppz and CoPc), we obtained CoPc-ndppzPMO consisting of cobalt phthalocyanine catalytic units (CoPc) embedded within the pore wall and dipyridyl-pyridazine moities (ndppz) in the pore channels. These chelating sites served as anchoring points for the immobilization of Ru- and Ir-based light-harvesting complexes, yielding robust hybrid architectures that integrate molecularly dispersed catalytic and photosensitizing components within a single mesostructured framework. Under visible-light irradiation, both CoPc-RuPMO and CoPc-IrPMO exhibited markedly enhanced CO_2 to CO conversion rates, reaching a level of activity exceeding 6.7 and 13 folds higher, respectively, compared to CoPc-ndppzPMO using homogeneous photosensitizers $[Ru(bpy)_2(dppz)](PF_6)_2$ or $[Ir(ppy)_2(dppz)]PF_6$ in solution. Interestingly, exposure of CoPc-ndppzPMO to $[Ru(bpy)_2Cl_2]$ led to in situ assembly of the photocatalyst, which mediated the photocatalytic reaction with a CO evolution rate comparable to that of pre-synthesized CoPc-RuPMO. Time-resolved photoluminescence studies demonstrated rapid electron transfer between photosensitizer and CoPc units, indicating their close spatial proximity within the PMO framework that plays a key role in facilitating photocatalysis. This work provides a rational approach for integrating photosensitizing and catalytic components in ordered hybrid frameworks, providing new insights into the design of efficient artificial photosynthetic systems for solar-driven CO_2 reduction.

Inorganic Chemistry Frontiers Accepted Manuscript

Author contributions

M.A.P.-L, R.R.-L, S. R, F. J. R.-S, and D. E. designed and directed the project. M. A. L.-P. and R. R.-L. carried out the synthesis, characterization, and catalytic studies of the materials. All authors participated in the drafting and revision of the manuscript.

Conflicts of interest

The authors declare no competing financial interest.

Data availability

Acknowledgements

The authors wish to acknowledge the financial support from the Spanish Ministry of Science and Innovation for projects PID2022/142657OB-I00 and PDC2022-133973-I00 and a FPI teaching and research fellowship (PREP2022-000024), Andalusian Regional Government (ProyExcel_00492 and FQM-346 group) and Feder Funds. R.R.L. acknowledges the Ramón Areces Foundation for a postdoctoral research fellowship (BEVP36A7462). S.R. acknowledges funding from EPSRC (EP/Y002911/1) and the Royal Society (International Exchange Grant IES\R1\231335). The technical staff from the Instituto Químico para la Energía y el Medioambiente (IQUEMA) and Servicio Central de Apoyo a la Investigación (SCAI) are also gratefully acknowledged. The authors acknowledge JBL Science facilities at the University of Lincoln (Joseph Banks Laboratories), UK, for the structural characterization (HRMS) of the target compounds.

References

1 Oh, J.-H.; Kug, J.-S.; An, S.-I.; Jin, F.-F.; McPhaden, M. J.; Shin, J. Emergent Climate Change Patterns Originating from Deep Ocean Warming in Climate Mitigation Scenarios. *Nat. Clim. Chang.* **2024**, *14* (3), 260–266.

2 Gabrielli, P.; Rosa, L.; Gazzani, M.; Meys, R.; Bardow, A.; Mazzotti, M.; Sansavini, G. Net-Zero Emissions Chemical Industry in a World of Limited Resources. *One Earth* **2023**, *6* (6), 682–704.

3 Davis, S. J.; Lewis, N. S.; Shaner, M.; Aggarwal, S.; Arent, D.; Azevedo, I. L.; Benson, S. M.; Bradley, T.; Brouwer, J.; Chiang, Y.-M. Net-Zero Emissions Energy Systems. *Science (1979).* **2018**, *360* (6396), eaas9793.

4 Peter, S. C. Reduction of CO_2 to Chemicals and Fuels: A Solution to Global Warming and Energy Crisis. *ACS Energy Lett.* **2018**, *3* (7), 1557–1561.

5 Anwar, M. N.; Fayyaz, A.; Sohail, N. F.; Khokhar, M. F.; Baqar, M.; Yasar, A.; Rasool, K.; Nazir, A.; Raja, M. U. F.; Rehan, M. CO_2 Utilization: Turning Greenhouse Gas into Fuels and Valuable Products. *J. Environ. Manage.* **2020**, *260*, 110059.

6 Zanatta, M. Materials for Direct Air Capture and Integrated CO_2 Conversion: Advancement, Challenges, and Prospects. *ACS Materials Au* **2023**, *3* (6), 576–583.

7 Kim, G. H.; Yang, J. W. Research Trends in CO_2 Utilization: Catalytic Strategies for Sustainable Energy and Environmental Protection. *Journal of CO_2 Utilization* **2025**, *101*, 103216.

8 Peng, W.; Nguyen, T. H. C.; Nguyen, D. L. T.; Wang, T.; Tran, T. V. T.; Le, T. H.; Le, H. K.; Grace, A. N.; Singh, P.; Raizadaa, P. A Roadmap towards the Development of Superior Photocatalysts for Solar-Driven CO_2-to-Fuels Production. *Renewable and Sustainable Energy Reviews* **2021**, *148*, 111298.

9 Nahar, S.; Zain, M. F. M.; Kadhum, A. A. H.; Hasan, H. A.; Hasan, M. R. Advances in Photocatalytic CO_2 Reduction with Water: A Review. *Materials* **2017**, *10* (6), 629.

10 Sun, Z.; Talreja, N.; Tao, H.; Texter, J.; Muhler, M.; Strunk, J.; Chen, J. Catalysis of Carbon Dioxide Photoreduction on Nanosheets: Fundamentals and Challenges. *Angew. Chem. Int. Ed.* **2018**, *57* (26), 7610–7627.

11 Abey, S. A.; Reis, N. M.; Emanuelsson, E. A. C.; Expósito, A. J. Harnessing Visible Light: Advanced Photocatalytic Strategies for Sustainable Environmental Reactions. *Chemical Engineering Journal* **2025**, *519*, 164951.

12 Biswas, S.; Dey, A.; Rahimi, F. A.; Barman, S.; Maji, T. K. Metal-Free Highly Stable and Crystalline Covalent Organic Nanosheet for Visible-Light-Driven Selective Solar Fuel Production in Aqueous Medium. *ACS Catal.* **2023**, *13* (9), 5926–5937.

13 Gil-Gavilan, D. G.; Rojas-Luna, R.; Amaro-Gahete, J.; Cosano, D.; Castillo-Rodriguez, M.; Esquivel, D.; Roy, S.; Ruiz, J. R.; Romero-Salguero, F. J. Zn–Cr LDH/Graphene Oxide Composites for Selective Photocatalytic CO_2 Reduction toward CO under Visible Light Irradiation. *Energy & Fuels* **2025**, *39* (19), 9134–9145.

14 Cheng, S.; Sun, Z.; Lim, K. H.; Gani, T. Z. H.; Zhang, T.; Wang, Y.; Yin, H.; Liu, K.; Guo, H.; Du, T. Emerging Strategies for CO_2 Photoreduction to CH_4: From Experimental to Data-driven Design. *Adv. Energy Mater.* **2022**, *12* (20), 2200389.

15 Chen, L.; Guo, Z.; Wei, X.-G.; Gallenkamp, C.; Bonin, J.; Anxolabéhère-Mallart, E.; Lau, K.-C.; Lau, T.-C.; Robert, M. Molecular Catalysis of the Electrochemical and Photochemical Reduction of CO_2 with Earth-Abundant Metal Complexes. Selective Production of CO vs HCOOH by Switching of the Metal Center. *J. Am. Chem. Soc.* **2015**, *137* (34), 10918–10921.

16 Elgrishi, N.; Chambers, M. B.; Wang, X.; Fontecave, M. Molecular Polypyridine-Based Metal Complexes as Catalysts for the Reduction of CO_2. *Chem. Soc. Rev.* **2017**, *46* (3), 761–796.

17 Dalle, K. E.; Warnan, J.; Leung, J. J.; Reuillard, B.; Karmel, I. S.; Reisner, E. Electro-and Solar-Driven Fuel Synthesis with First Row Transition Metal Complexes. *Chem. Rev.* **2019**, *119* (4), 2752–2875.

18 Gholamkhass, B.; Mametsuka, H.; Koike, K.; Tanabe, T.; Furue, M.; Ishitani, O. Architecture of Supramolecular Metal Complexes for Photocatalytic CO_2 Reduction: Ruthenium− Rhenium Bi-and Tetranuclear Complexes. *Inorg. Chem.* **2005**, *44* (7), 2326–2336.

19 Wang, X.; Meng, S.; Chen, J.; Wang, H.; Wang, Y.; Zhou, S.; Li, X.; Liao, R.; Tung, C.; Wu, L. Mechanistic Insights Into Iron (II) Bis (Pyridyl) Amine-Bipyridine Skeleton for Selective CO_2 Photoreduction. *Angew. Chem. Int. Ed.* **2021**, *60* (50), 26072–26079.

20 Wang, J. W.; Jiang, L.; Huang, H. H.; Han, Z.; Ouyang, G. Rapid Electron Transfer via Dynamic Coordinative Interaction Boosts Quantum Efficiency for Photocatalytic CO_2 Reduction. *Nat. Commun.* **2021**, *12* (1). https://doi.org/10.1038/s41467-021-24647-y.

21 Schneider, J.; Matsuoka, M.; Takeuchi, M.; Zhang, J.; Horiuchi, Y.; Anpo, M.; Bahnemann, D. W. Understanding TiO_2 Photocatalysis: Mechanisms and Materials. *Chem. Rev.* **2014**, *114* (19), 9919–9986.

View Article Online DOI: 10.1039/D5QI01803J

Inorganic Chemistry Frontiers Accepted Manuscript

Open Access Article. Published on 22 June 2026. Downloaded on 6/23/2026 3:24:23 AM. This article is licensed under a Creative Commons Attribution-NonCommercial 3.0 Unported Licence.

Please do not adjust margins

View Article Online
DOI: 10.1039/D6QI00603J

22 Loumissi, T.; Ishii, R.; Hara, K.; Oyumi, T.; Abe, I.; Li, C.; Zhang, H.; Hirayama, R.; Niki, K.; Itoi, T. Exchange of CO_2 with CO as Reactant Switches Selectivity in Photoreduction on Co− ZrO_2 from C_{1-3} Paraffin to Small Olefins. *Angewandte Chemie* **2024**, *136* (51), e202412090.

23 Xu, F.; Meng, K.; Cheng, B.; Wang, S.; Xu, J.; Yu, J. Unique S-Scheme Heterojunctions in Self-Assembled TiO_2/$CsPbBr_3$ Hybrids for CO_2 Photoreduction. *Nat. Commun.* **2020**, *11* (1), 4613.

24 Reguero, M.; Claver, C.; Carrilho, R. M. B.; Masdeu-Bultó, A. M. Immobilized Molecular Catalysts for CO_2 Photoreduction. *Adv. Sustain. Syst.* **2022**, *6* (6), 2100493.

25 Liang, H.-P.; Acharjya, A.; Anito, D. A.; Vogl, S.; Wang, T.-X.; Thomas, A.; Han, B.-H. Rhenium-Metalated Polypyridine-Based Porous Polycarbazoles for Visible-Light CO_2 Photoreduction. *ACS Catal.* **2019**, *9* (5), 3959–3968.

26 Yin, H.-Q.; Zhang, Z.-M.; Lu, T.-B. Ordered Integration and Heterogenization of Catalysts and Photosensitizers in Metal-/Covalent-Organic Frameworks for Boosting CO_2 Photoreduction. *Acc. Chem. Res.* **2023**, *56* (19), 2676–2687.

27 Karmakar, S.; Barman, S.; Rahimi, F. A.; Maji, T. K. Covalent Grafting of Molecular Photosensitizer and Catalyst on MOF-808: Effect of Pore Confinement toward Visible Light-Driven CO_2 Reduction in Water. *Energy Environ. Sci.* **2021**, *14* (4), 2429–2440.

28 Ali, O.; Das, A.; Jana, A.; Mandal, S.; Adalder, A.; Maity, B.; Bhunia, A. Functional Integration of [Ir(Ppy)$_2$(H_2Dcbpy)] and a Molecular Nickel Complex into Metal-Organic Frameworks for Photocatalytic CO_2 Reduction. *ChemCatChem* **2025**, *17* (18), e00844.

29 Li, X.-S.; He, Y.-J.; Chen, J.; Li, Q.-Q.; Liu, P.; Li, J.-L. Recent Advances in Rational Design, Synthesis and Application of Metal–Organic Frameworks as Visible-Light-Driven Photocatalysts. *Inorg. Chem. Front.* **2024**, *11* (20), 6794–6852.

30 Gong, L.-J.; Liu, L.-Y.; Zhao, S.-S.; Yang, S.-L.; Si, D.-H.; Wu, Q.-J.; Wu, Q.; Huang, Y.-B.; Cao, R. Rapid Charge Transfer in Covalent Organic Framework via Through-Bond for Enhanced Photocatalytic CO_2 Reduction. *Chemical Engineering Journal* **2023**, *458*, 141360.

31 Nguyen, H. L.; Alzamly, A. Covalent Organic Frameworks as Emerging Platforms for CO_2 Photoreduction. *ACS Catal.* **2021**, *11* (15), 9809–9824.

32 Van Der Voort, P.; Esquivel, D.; De Canck, E.; Goethals, F.; Van Driessche, I.; Romero-Salguero, F. J. Periodic Mesoporous Organosilicas: From Simple to Complex Bridges; a Comprehensive Overview of Functions, Morphologies and Applications. *Chem. Soc. Rev.* **2013**, *42* (9), 3913–3955.

33 Takeda, H.; Ohashi, M.; Tani, T.; Ishitani, O.; Inagaki, S. Enhanced Photocatalysis of Rhenium (I) Complex by Light-Harvesting Periodic Mesoporous Organosilica. *Inorg. Chem.* **2010**, *49* (10), 4554–4559.

34 Zhang, S.; Li, M.; Qiu, W.; Han, J.; Wang, H.; Liu, X. Heterogeneous Molecular Rhenium Catalyst for CO_2 Photoreduction with High Activity and Tailored Selectivity in an Aqueous Solution. *Appl. Catal. B* **2019**, *259*, 118113.

35 Kuramochi, Y.; Sekine, M.; Kitamura, K.; Maegawa, Y.; Goto, Y.; Shirai, S.; Inagaki, S.; Ishida, H. Photocatalytic CO_2 Reduction by Periodic Mesoporous Organosilica (PMO) Containing Two Different Ruthenium Complexes as Photosensitizing and Catalytic Sites. *Chemistry–A European Journal* **2017**, *23* (43), 10301–10309.

36 Waki, M.; Maegawa, Y.; Hara, K.; Goto, Y.; Shirai, S.; Yamada, Y.; Mizoshita, N.; Tani, T.; Chun, W.-J.; Muratsugu, S. A Solid Chelating Ligand: Periodic Mesoporous Organosilica Containing 2, 2′-Bipyridine within the Pore Walls. *J. Am. Chem. Soc.* **2014**, *136* (10), 4003–4011.

37 Waki, M.; Yamanaka, K.; Shirai, S.; Maegawa, Y.; Goto, Y.; Yamada, Y.; Inagaki, S. Re (Bpy)$(CO)_2$Cl Immobilized on Bipyridine-Periodic Mesoporous Organosilica for Photocatalytic CO_2 Reduction. *Chemistry–A European Journal* **2018**, *24* (15), 3846–3853.

38 Waki, M.; Ikai, M.; Goto, Y.; Maegawa, Y.; Inagaki, S. Re (Bpy)$(CO)_2$Cl Immobilized on Bipyridine Organosilica Nanotubes for Photocatalytic CO_2 Reduction. *Eur. J. Inorg. Chem.* **2021**, *2021* (17), 1624–1631.

39 Rojas-Luna, R.; Castillo-Rodríguez, M.; Ruiz, J. R.; Jiménez-Sanchidrián, C.; Esquivel, D.; Romero-Salguero, F. J. Ru-and Ir-Complex Decorated Periodic Mesoporous Organosilicas as Sensitizers for Artificial Photosynthesis. *Dalton Transactions* **2022**, *51* (48), 18708–18721.

40 Rojas-Luna, R.; Romero-Salguero, F. J.; Esquivel, D.; Roy, S. Manipulating the Coordination Structure of Molecular Cobalt Sites in Periodic Mesoporous Organosilica for CO_2 Photoreduction. *ACS Appl. Energy Mater.* **2024**, *7* (14), 5924–5936.

41 Rojas-Luna, R.; Amaro-Gahete, J.; Konar, S.; Romero-Salguero, F. J.; Esquivel, D.; Roy, S. Immobilisation of a Molecular Iridium Complex on Periodic Mesoporous Organosilica for Heterogeneous Water Oxidation Catalysis. *Sustain. Energy Fuels* **2025**, *9* (11), 2961–2972.

42 Navarro, M. A.; Sain, S.; Wünschek, M.; Pichler, C. M.; Romero-Salguero, F. J.; Esquivel, D.; Roy, S. Solar Driven CO_2 Reduction with a Molecularly Engineered Periodic Mesoporous Organosilica Containing Cobalt Phthalocyanine. *Nanoscale* **2023**, *15* (5), 2114–2121.

43 Palmer, R. A.; Piper, T. S. 2, 2′-Bipyridine Complexes. I. Polarized Crystal Spectra of Tris (2, 2′-Bipyridine) Copper (II),-Nickel (II),-Cobalt (II),-Iron (II), and-Ruthenium (II). *Inorg. Chem.* **1966**, *5* (5), 864–878.

44 Lowry, M. S.; Hudson, W. R.; Pascal, R. A.; Bernhard, S. Accelerated Luminophore Discovery through Combinatorial Synthesis. *J. Am. Chem. Soc.* **2004**, *126* (43), 14129–14135.

45 Guan, B.; Cui, Y.; Ren, Z.; Qiao, Z.; Wang, L.; Liu, Y.; Huo, Q. Highly Ordered Periodic Mesoporous Organosilica Nanoparticles with Controllable Pore Structures. *Nanoscale* **2012**, *4* (20), 6588–6596.

46 Kirren, P.; Barka, L.; Rahmani, S.; Bondon, N.; Donzel, N.; Trens, P.; Bessière, A.; Raehm, L.; Charnay, C.; Durand, J.-O. Periodic Mesoporous Organosilica Nanoparticles for CO_2 Adsorption at Standard Temperature and Pressure. *Molecules* **2022**, *27* (13), 4245.

47 Verma, D.; Dash, R.; Katti, K. S.; Schulz, D. L.; Caruso, A. N. Role of Coordinated Metal Ions on the Orientation of Phthalocyanine Based Coatings. *Spectrochim. Acta A Mol. Biomol. Spectrosc.* **2008**, *70* (5), 1180–1186.

48 Zanganeh, F.; Yamini, Y.; Khataei, M. M.; Badiei, A. Ethane-Bridge Periodic Mesoporous Organosilica Materials as a Novel Fiber Coating in Headspace Solid-Phase Microextraction of Phthalate Esters from Saliva and PET Container Samples. *Anal. Bioanal. Chem.* **2022**, *414* (6), 2285–2296.

49 Klyamer, D. D.; Basova, T. V; Krasnov, P. O.; Sukhikh, A. S. Effect of Fluorosubstitution and Central Metals on the Molecular Structure and Vibrational Spectra of Metal Phthalocyanines. *J. Mol. Struct.* **2019**, *1189*, 73–80.

50 Kumar, T. M. S.; Kumar, N. Y. P.; Reddy, K. R. V.; Chandrakala, K. B.; Arunkumar, L.; Vidyasagar, C. C. Novel

Open Access Article. Published on 22 June 2026. Downloaded on 6/23/2026 3:24:23 AM.
This article is licensed under a Creative Commons Attribution-NonCommercial 3.0 Unported Licence.

Inorganic Chemistry Frontiers Accepted Manuscript

This journal is © The Royal Society of Chemistry 20xx

Please do not adjust margins

View Article Online
DOI: 10.1039/D6QI00603E

Schiff Base Cobalt (Ii) Phthalocyanine with Appliance of MWCNTs on GCE: Enhanced Electrocatalytic Activity Behaviour of α-Amino Acids. *RSC Adv.* **2021**, *11* (27), 16736–16746.

51 Spitler, E. L.; Dichtel, W. R. Lewis Acid-Catalysed Formation of Two-Dimensional Phthalocyanine Covalent Organic Frameworks. *Nat. Chem.* **2010**, *2* (8), 672–677.

52 Auras, F.; Li, Y.; Löbermann, F.; Döblinger, M.; Schuster, J.; Peter, L. M.; Trauner, D.; Bein, T. A Zinc Phthalocyanine Based Periodic Mesoporous Organosilica Exhibiting Charge Transfer to Fullerenes. *Chemistry–A European Journal* **2014**, *20* (46), 14971–14975.

53 Hoogenboom, R.; Kickelbick, G.; Schubert, U. S. Synthesis and Characterization of Novel Substituted 3, 6-Di (2-pyridyl) Pyridazine Metal-Coordinating Ligands. *European J. Org. Chem.* **2003**, *2003* (24), 4887–4896.

54 DeWitt, C. H.; Heidbreder, A. D.; Hancock, G. W.; Bhattacherjee, A. Investigation of Vibrational Cooling in a Photoexcited Dichloro-Ruthenium Charge Transfer Complex Using Transient Electronic Absorption Spectroscopy. *J. Phys. Chem. A* **2025**, *129* (9), 2265–2274.

55 Filevich, O.; Zayat, L.; Baraldo, L. M.; Etchenique, R. Long Wavelength Phototriggering: Ruthenium-Based Caged Compounds. In *Luminescent and Photoactive Transition Metal Complexes as Biomolecular Probes and Cellular Reagents*; Springer, 2014; pp 47–68.

56 Lafolet, F.; Welter, S.; Popović, Z.; De Cola, L. Iridium Complexes Containing P-Phenylene Units. The Influence of the Conjugation on the Excited State Properties. *J. Mater. Chem.* **2005**, *15* (27–28), 2820–2828.

57 Waki, M.; Shirai, S.; Yamanaka, K.; Maegawa, Y.; Inagaki, S. Heterogeneous Water Oxidation Photocatalysis Based on Periodic Mesoporous Organosilica Immobilizing a Tris (2, 2′-Bipyridine) Ruthenium Sensitizer. *RSC Adv.* **2020**, *10* (24), 13960–13967.

58 Roy, S.; Reisner, E. Visible-light-driven CO_2 Reduction by Mesoporous Carbon Nitride Modified with Polymeric Cobalt Phthalocyanine. *Angew. Chem. Int. Ed.* **2019**, *58* (35), 12180–12184.

59 Agnès, C.; Arnault, J.-C.; Omnès, F.; Jousselme, B.; Billon, M.; Bidan, G.; Mailley, P. XPS Study of Ruthenium Tris-Bipyridine Electrografted from Diazonium Salt Derivative on Microcrystalline Boron Doped Diamond. *Physical Chemistry Chemical Physics* **2009**, *11* (48), 11647–11654.

60 Xu, N.; Diao, Y.; Xu, Z.; Ke, H.; Zhu, X. Covalent Triazine Frameworks Embedded with Ir Complexes for Enhanced Photocatalytic Hydrogen Evolution. *ACS Appl. Energy Mater.* **2022**, *5* (6), 7473–7478.

61 Tinker, L. L.; Bernhard, S. Photon-Driven Catalytic Proton Reduction with a Robust Homoleptic Iridium (III) 6-Phenyl-2, 2′-Bipyridine Complex (Ir (C/\N/\N)$^{2+}$). *Inorg. Chem.* **2009**, *48* (22), 10507–10511.

62 Tinker, L. L.; McDaniel, N. D.; Curtin, P. N.; Smith, C. K.; Ireland, M. J.; Bernhard, S. Visible Light Induced Catalytic Water Reduction without an Electron Relay. *Chemistry–A European Journal* **2007**, *13* (31), 8726–8732.

63 Kuramochi, Y.; Ishitani, O. Iridium (III) 1-Phenylisoquinoline Complexes as a Photosensitizer for Photocatalytic CO_2 Reduction: A Mixed System with a Re (I) Catalyst and a Supramolecular Photocatalyst. *Inorg. Chem.* **2016**, *55* (11), 5702–5709.

64 Liu, G.; Wang, Y.; Zhou, Y.; Cao, J.; Yuan, M.; Lv, H. Phosphorous Doped G-C_3N_4 Supported Cobalt Phthalocyanine: An Efficient Photocatalyst for Reduction of CO_2 under Visible-Light Irradiation. *J. Colloid Interface Sci.* **2021**, *594*, 658–668.

65 Rong, J.; Xu, Q.; Han, J.; Ren, K.; Zhang, J.; Zhao, X.; She, P.; Qin, J.-S.; Rao, H. In Situ Construction of Cobalt Phthalocyanine Covalent Organic Polymer on Mesoporous Graphitic Carbon Nitride for Boosting Photocatalytic CO_2 Reduction. *Chemical Engineering Journal* **2025**, *507*, 160814.

66 Stanley, P. M.; Thomas, C.; Thyrhaug, E.; Urstoeger, A.; Schuster, M.; Hauer, J.; Rieger, B.; Warnan, J.; Fischer, R. A. Entrapped Molecular Photocatalyst and Photosensitizer in Metal–Organic Framework Nanoreactors for Enhanced Solar CO_2 Reduction. *ACS Catal.* **2021**, *11* (2), 871–882.

67 Elcheikh Mahmoud, M.; Audi, H.; Assoud, A.; Ghaddar, T. H.; Hmadeh, M. Metal–Organic Framework Photocatalyst Incorporating Bis (4′-(4-Carboxyphenyl)-Terpyridine) Ruthenium (II) for Visible-Light-Driven Carbon Dioxide Reduction. *J. Am. Chem. Soc.* **2019**, *141* (17), 7115–7121.

68 Zhang, X.; Cibian, M.; Call, A.; Yamauchi, K.; Sakai, K. Photochemical CO_2 Reduction Driven by Water-Soluble Copper (I) Photosensitizer with the Catalysis Accelerated by Multi-Electron Chargeable Cobalt Porphyrin. *ACS Catal.* **2019**, *9* (12), 11263–11273.

69 Ma, F.; Luo, Z.-M.; Wang, J.-W.; Ouyang, G. Highly Efficient, Noble-Metal-Free, Fully Aqueous CO_2 Photoreduction Sensitized by a Robust Organic Dye. *J. Am. Chem. Soc.* **2024**, *146* (26), 17773–17783.

70 Hu, X.; Rønne, M. H.; Pedersen, S. U.; Skrydstrup, T.; Daasbjerg, K. Enhanced Catalytic Activity of Cobalt Porphyrin in CO_2 Electroreduction upon Immobilization on Carbon Materials. *Angew. Chem. Int. Ed.* **2017**, *56* (23), 6468–6472.

71 Wang, J.-W.; Zhang, X.; Velasco, L.; Karnahl, M.; Li, Z.; Luo, Z.-M.; Huang, Y.; Yu, J.; Hu, W.; Zhang, X. Precious-Metal-Free CO_2 Photoreduction Boosted by Dynamic Coordinative Interaction between Pyridine-Tethered Cu (I) Sensitizers and a Co (II) Catalyst. *JACS Au* **2023**, *3* (7), 1984–1997.

Open Access Article. Published on 22 June 2026. Downloaded on 6/23/2026 3:24:23 AM.
This article is licensed under a Creative Commons Attribution-NonCommercial 3.0 Unported Licence.

Inorganic Chemistry Frontiers Accepted Manuscript

View Article Online
DOI: 10.1039/D6QI00603E

Data Availability Statement

Data for this article, including XRD, N_2 sorption measurements, FT-IR, Raman, UV-vis, XPS and TRPL measurements are available at Zenodo at https://doi.org/10.5281/zenodo.18224598

Open Access Article. Published on 22 June 2026. Downloaded on 6/23/2026 3:24:23 AM.
This article is licensed under a Creative Commons Attribution-NonCommercial 3.0 Unported Licence.

Inorganic Chemistry Frontiers Accepted Manuscript